AA13 - CFD Modeling of Gas Suspension Calciner in an Alumina Refinery

Sai Hitesh Bhandaru[1], Kumaresan Thangaraj[2], Vilas Tathavadkar[3], Subha Banerjee[4], Kiran Kumar Kondala[5] and Kausikisaran Misra[6]
1. Scientist
2. Lead Scientist (Domain Leader)
3. Senior Vice-president (Function Head)
Aditya Birla Science and Technology Company Pvt. Ltd, Navi Mumbai, Maharashtra, India
4. Senior Engineer
5. Senior Manager
6. General Manager – Technical
Utkal Alumina International Limited, Rayagada, Odisha, India
Corresponding Author: kumaresan.t@adityabirla.com

Abstract

Calcination of gibbsite to alumina is an important energy intensive final stage of Bayer alumina refinery process. Approximately, 30 % of the total energy consumption is alone used for the calcination stage. Thus, improvement of energy efficiency plays a crucial role in minimizing cost of production and emissions. The aim of this study is to investigate combustion efficiency of heavy fuel oil (HFO) atomized with steam inside the gas suspension calciner of alumina refinery. The combustion model was developed using species transport model with addition of all possible combustion reactions. Discrete phase lagrangian approach model was incorporated for studying HFO and alumina hydrate particle trajectories in combustion and holding vessel zones. Turbulence has been modeled using SST – K-ω turbulence model and P1 method was used for accounting radiative heat transfer equation. Post combustion efficiency investigation with respect to the mole fractions of carbon dioxide, carbon monoxide, unburnt O_2 emissions, this work also aims to focus on introducing routes (such as optimization of Air to fuel ratio) for reduction of fuel consumption less than the design consumption and to build an optimum curve for best fuel efficiency with respect to throughput satisfying operation limits.

Keywords: Alumina calcination, alpha alumina, combustion efficiency, CFD modeling, fuel consumption.

1. Introduction

Bauxite ore consists of gibbsite, boehmite, diaspore, bayerite, nordstrandite, tohdite, kaolinite and doyleite as aluminum containing phases along with calcium, iron and silica phases viz., hematite, anatase and quartz. Among the minerals present in bauxite, gibbsite, bayerite, nordstrandite and doyleite are aluminum tri-hydroxides while boehmite, diaspore and tohdite are aluminum oxide hydroxides. The detailed alumina minerals with their compositions depicted in Table 1 were given by Wefers et al., (1987) [1]. Properties, minerology, type, amount of alumina content and other impurities vary widely in bauxite depending on its geographical location. Aluminum containing phases in bauxite are widely used to produce smelter grade, specialty grade and high purity alumina in alumina refineries across the globe using conventional Bayer Alumina process. Along with these applications, alumina also finds applications as a flame retardant and paper additive while, boehmite is used as a catalyst support and in the production of ceramic pieces [2], [3]. Due to these wide applications and properties, alumina has achieved a great significance industrially and in the new technology development.

Table 1. Comparison of different oxides of Aluminum [1].

S.No	Name of alumina mineral	Chemical composition	Crystallographic formula
1	Gibbsite	Aluminum tri-hydroxide	γ-$Al(OH)_3$
2	Bayerite	Aluminum tri-hydroxide	α-$Al(OH)_3$
3	Nordstrandite	Aluminum tri-hydroxide	$Al(OH)_3$
4	Boehmite	Aluminum mono-hydroxide	γ-AlOOH
5	Diaspore	Aluminum mono-hydroxide	α-AlOOH
6	Corundum	Aluminum oxide	α-Al_2O_3

Among these minerals, gibbsite ($Al(OH)_3$) is the pre-dominant phase available in the Eastern Ghats bauxite present at Utkal Alumina International Limited (UAIL). This mineral composite is widely used for production of smelter grade alumina from raw bauxite ore which is an energy intensive process that uses substantial amounts of caustic soda for extraction of gibbsite.
In alumina refineries, bauxite ore is processed using the Bayer process to extract alumina tri-hydroxide (gibbsite). Calcination of gibbsite or $Al(OH)_3$, to alumina occur via an endothermic thermal decomposition reaction which is given by

$$2Al(OH)_3 \xrightarrow{1000°C} Al_2O_3 + 3H_2O, \quad \Delta H° = +185.2 \text{ kJ/mol} \tag{1}$$

Equation 1 which seems to be a simple one step reaction happens at over 1000 °C to produce desirable alumina phase with an LOI less than 1%. Alumina calcination process involves various stages viz., unbound moisture removal, phase and structural transformations in which hydroxides are converted to oxides. Residual hydroxide content starts to decrease with temperature and time in a calcination process. Most of the reduction in free moisture present in the feed hydrate was observed in temperatures lower than 250 °C after which at a reduced rate of LOI, phase and structural transformations takes place.

Phase transformations play a crucial role in an alumina calcination process for producing desirable alumina phase. During the calcination process, alumina has a significance of existing in various metastable forms including γ, χ, κ, δ, η, θ and in the final stable α-alumina phase. The reaction pathway to several alumina phases are majorly characterized by particle sizes and heating rates. On-set of phase transformation to alumina mono hydroxide (Boehmite) from gibbsite starts at temperatures lower than 250 °C after which several phase transformations based on heating rates and particle sizes to χ and desirable γ-alumina takes place at temperatures between 300 to 800 °C. Stable alpha alumina formation occurs at temperatures greater than 1000 °C.

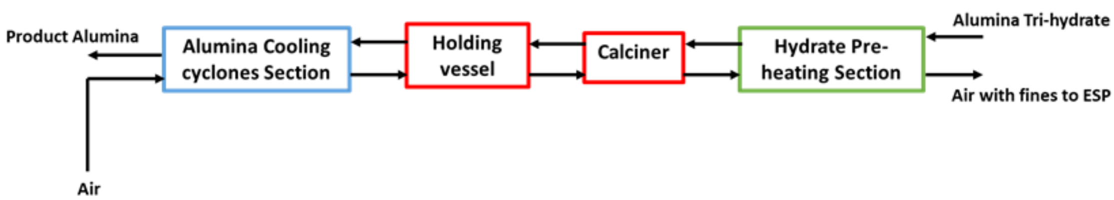

Figure 1. Block diagram of calcination process in an alumina refinery.

In modern day Gas suspension calciners (GSC), gibbsite particles were fed into a series of pre-heaters maintained at around 300-500 °C for removing moisture and initiating the conversion of aluminium tri-hydroxide to mono-hydrated alumina (boehmite) and transition alumina. In the calciner furnace and holding vessel sections, production to a desirable smelter grade alumina is carried out. Post calcination, heat associated with alumina is recovered using a series of cooling cyclones where air gets pre-heated as shown in Figure 1.

Approximately, 30 % of the energy is solely utilized by the calcination process by combusting heavy fuel oil having a gross calorific value of 10500 Kcal/Kg with air in a gas suspension calciner. The control on calcination process for reduction of specific heavy fuel oil consumption and formation of desirable alumina phase should be carefully done due to very high sensitivity of the process to any changes to the design of process equipment key operational parameters. This would directly have an impact on the quality of alumina and cost efficiency which in turn would affect the performance of the plant. Nevertheless, in the current study the focus is mainly to assess and improve the process efficiency of the existing calcination design.

A numerical simulation would provide better understanding of physico-chemical events inside calcination process which is equally complicated for a calcination process of alumina due to several simultaneous physical processes coupled together involving flow of air and hydrate particles, combustion of fuel oil [4]. All these phenomena must be considered in one single model to obtain accurate and desirable results at different variations of Air to fuel ratio and hydrate feed rate. Figure 2 shown below depicts the CFD model developed for a gas suspension calciner. This numerical model captures the combustion behavior, flow and transport processes occurring in an alumina calciner. The model is based on solving the Navier-Stokes equation for the flow of air, Lagrangian approach for discrete phase particles using Ansys CFD.

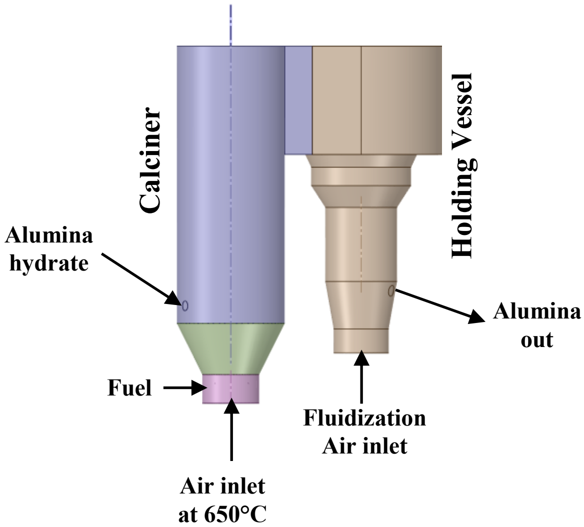

Figure 2. Schematic of CFD model for a calciner with holding vessel.

This work covers analysis of the variables majorly effecting the specific heavy fuel oil consumption from the plant data, modeling approach to simulate combustion efficiency of heavy fuel oil and fluidization of particles within calciner and holding vessel and phase transformational analysis using different characterization techniques to understand and validate the CFD results on the phases formed from alumina hydrate at different temperatures, heating rates and particle size distributions.

2. Model Description

2.1. CFD Simulation

There is limited literature available specific to CFD simulation of the alumina calcination process. CFD modeling of the gas temperatures and solids flow pattern in a single furnace of an alumina calciner to assess the combustion of heavy fuel oil and the effect of temperature upon addition of solid feed was carried out by researchers [4]. The geometry was created using Design Modeler Ansys 2019 R2 and the polyhedra meshing was carried out using Fluent mesh 2019 R2 and numerical simulations are carried out using ANSYS-Fluent 2019 R2.

The geometry of the 3D model consists of cylindrical and conical sections to make a combination of calciner and holding vessel having three inlets one for hydrate injection, one for combustion and transportation air into calciner and final inlet for fluidization air into holding vessel and one outlet at the bottom of holding vessel. All geometric data and boundary conditions were collected from Utkal Alumina International Limited (UAIL), Rayagada, Orissa.

From the geometry, it was assumed to have a strong swirl flow and to track particles near wall and accurately capture wall effects, SST k-ω turbulence model was used. The combustion model was developed using species transport model with addition of all possible combustion reactions. Discrete phase Eularian-lagrangian approach model was incorporated for studying Heavy Fuel Oil (HFO) and alumina hydrate droplet/particle trajectories. P1 method using the "particle radiation interaction" was used for accounting radiative heat transfer equation. Radiation is majorly dominant in the burner region where fuel droplets burns and evaporates quickly. P1 model has an advantage of good accuracy and properly accounts for radiation between air and hydrate particles in the calciner. Fuel oil droplet size was assumed to be uniform (100µm) from the atomizer with steam.

2.1.1. Eulerian Gaseous Phase Equations

Continuity equation

$$\frac{\partial \rho}{\partial t} + \nabla.(\rho.u) = 0 \tag{2}$$

Momentum equation

$$\frac{\partial}{\partial t}(\rho u) + \nabla.(\rho u u) = -\nabla p + \nabla.(\tau) + \rho g + F \tag{3}$$

Where p is static pressure, ρg and F are gravitational and external body forces and τ is stress tensor given by,

$$\tau = \mu \left(\nabla u + (\nabla u)^T - \frac{2}{3}\delta \nabla \bullet u \right) \tag{4}$$

Energy equation between solid phase (A) and gas phase (B) is given by

$$\frac{\partial}{\partial t}(\alpha_A \rho_A h_A) + \nabla.(\alpha_A \rho_A \gamma_i h_A) = \alpha_A \frac{\partial P_A}{\partial t} + t_A \nabla \mu_A - \nabla.q_A + \sum_{j=1}^{n} Q_{BA} + S_A \tag{5}$$

where, α_A is the volume fraction of particles in the calciner, t_A is the stress tensor given by eq 3, P_A is the pressure of particles in phase 'A', h_A and q_A are enthalpy and heat flux of species in phase A, Q_{BA} is the rate at which energy is getting transferred from gas phase B to solid phase A and Si is the source term due to homogenous combustion reactions. Rate of energy transfer is given by,

$$Q_{BA} = h_{BA}(T_B - T_A) \tag{6}$$

where, h_{BA} is the heat transfer coefficient between gas phase B and solid phase A and T is the temperature of different phases. Gunn model was developed to account and calculate the heat transfer between gas phase (air) and particles which is given by [5],

$$h_{BA} = \frac{6k_B\alpha_A\alpha_B Nu_A}{d_{pA}^2} \tag{7}$$

where, k_B is thermal conductivity of gas phase and Nu_A is the Nusselt number of particle phase

$$Nu_A = (7 - 10\alpha_B + 5\alpha_B^2)\left(1 + 0.7\, Re_A^{0.2}.Pr^{0.33}\right) + (1.33 - 2.4\alpha_B + 1.2\alpha_B^2)Re_i^{0.7}Pr^{0.33} \tag{8}$$

where, Re_i is the Reynold's number at corresponding particle diameter and Pr is Prandtl number.

2.1.2. Discrete Phase Model (DPM)

Trajectory of Heavy fuel oil droplets and hydrate particles, interaction of discrete phase with continuous were calculated from equation of motion [6] [7]

$$\frac{dUp}{dt} = F_D(U - Up) + gi * \frac{\rho_p - \rho}{\rho} + fi \tag{9}$$

where subscript p indicates hydrate/alumina particle

For spherical particles, drag force, F_D is given by

$$F_D = \frac{3\mu C_D * Re}{4\rho_p Dp^2} \tag{10}$$

Where C_D is given by

$$C_D = \alpha_1 + \frac{\alpha_2}{Re} + \frac{\alpha_3}{Re} \tag{11}$$

Constants α1, α2 and α3 are developed by Morsi et al., [6]

2.1.3. Particle Size Distribution

Particle size distribution for hydrate follow Rosin-Rammler distribution given by

$$M_D = \exp(-\left({}^{D}/_{D_o}\right)^n) \tag{11a}$$

Where n is given by

$$n = \frac{\ln(lnM_D)}{\ln({}^{D}/_{D_o})} \tag{12}$$

2.1.4. Species Transport Equation

Homogeneous chemical reactions for combustion were given under species transport mechanism. The species transport model for homogeneous reactions containing volume fraction α, source term for mass transfer and rate of reaction for a species i in a gaseous phase j is given by,

$$\frac{\partial}{\partial t}\left(\rho_j \alpha_j Y_i^j\right) + \nabla.\left(\rho_j \alpha_j u_j Y_i^j\right) = -\nabla.\alpha_j J_i^j + \alpha_j R_i^j + \alpha_j S_i^j \tag{13}$$

where, Yi is the mass fraction of species i in gaseous phase j, R_i^j is the rate of homogenous chemical reaction in gaseous phase j, S_i^j is the source term from the discrete phase droplets in gaseous phase j and J_i^j is the diffusive flux occurred in gas phase j due to concentration gradient, which, for a turbulent flow is given by,

$$J_i^j = -\left(\rho D_{i,j} + \frac{\mu_t}{Sc}\right)\nabla Y_i \tag{14}$$

$D_{i,j}$ is coefficient of diffusion for species i in a gas phase j, μ_t is turbulent viscosity and Sc is Schmidt number for a turbulent flow. These values were proposed by Versteeg et al. [8].

2.1.5. Combustion Model

Heavy fuel oil in a calciner initially gets heated followed by vaporization of droplets which then finally participates in a combustion reaction. When oil droplets reach the temperature of vaporization, vapors of HFO are released with a rate based on the concentration gradient of oil vapor between droplet surface $C_{i,s}$ and gaseous phase (air), $C_{i,g}$. The molar flux is thus given by,

$$N_i = k_c(C_{i,s} - C_{i,g}) \tag{15}$$

where, k_c is the mass transfer coefficient due to concentration gradient.
Post diffusion between oil droplet surface to gas phase, a homogeneous combustion reaction takes place. A generalized form of the reaction to yield major combustion products is as given below

$$C_xH_yO_z + O_2 \rightarrow CO_2 + H_2O \tag{16}$$

$$C_xH_yO_z + O_2 \rightarrow CO + H_2O \tag{17}$$

2.1.6. Radiation Model

Along with convective heat transfer, radiation is the pre-dominating heat transfer phenomenon occurring inside the calciner after combustion process due to higher temperature. To capture the effects of droplets from heavy furnace oil (HFO) inside the calciner, P1 model was used for calculation of amount of radiation from HFO droplets into the air flow carrying hydrate particles. The corresponding equation for the radiative heat transfer is given by,

$$-\nabla q_r = -4\pi\left(a\frac{\sigma T}{\pi} + E_p\right) + \left(a + a_p\right)G \tag{18}$$

where, q_r is the radiative heat transfer flux, a is heat absorption coefficient, σ is Stephen Boltzmann constant which is 5.67 x 10^{-8} W/m^{2}K^4, E_p is coefficient of equivalent emission, a_p is coefficient of equivalent absorption and G is the radiation of incidence. Coefficients of equivalent emission and absorption are calculated in FLUENT during particle tracking using the following equations

$$E_p = \lim_{V \to 0} \sum_{n=1}^{N} \varepsilon_{pn} A_{pn} \frac{\sigma T_{pn}^4}{\pi V} \tag{19}$$

$$a_p = \lim_{V \to 0} \sum_{n=1}^{N} \varepsilon_{pn} \frac{A_{pn}}{\pi V} \tag{20}$$

2.2. Calciner Model

Calcination of gibbsite or aluminium tri-hydroxide to alumina occur via an endothermic thermal decomposition reaction which is given by

$$2Al(OH)_3 \xrightarrow{1000\,°C} Al_2O_3 + 3H_2O,\ \Delta H^o = +185.2 \text{ kJ/mol} \tag{21}$$

Gas suspension calciner furnace as shown in Figure 2, comprises of a series of cylindrical and conical sections having four inlets in total with 5 burners for injection of heavy fuel oil (HFO) droplets having a diameter of 0.0278 m each, inlets for air enter through a diameter of 3.25 m, fluidization air enter through 3.59 m diameter and feed hydrate enters through a diameter of 0.56 m near the bottom part of calciner and holding vessel. The calcined alumina product exits through one outlet having a diameter of 0.63 m near the bottom cylindrical section of the holding vessel.

The computational model is built with a polyhedral mesh with a total of 1 080 000 cells. Figure 3 shown below depicts the mesh built using Fluent. Mass flow inlet and pressure outlet type boundary condition was selected. FLUENT solver was used to incorporate all the boundary conditions, several models viz., Two way coupled discrete phase model, species transport model, turbulence model etc., to incorporate chemical reactions, particle injections.

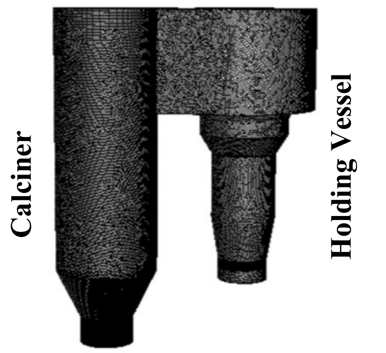

Figure 3. 3D polyhedral mesh of gas suspension calciner.

All the necessary data on building geometry, physics setup including all the inlet and boundary conditions were collected from Utkal Alumina International Limited (UAIL), Rayagada, Orissa. Table 2 and 3 shown below represent the boundary conditions for air to fuel ratios 22.8 and 26.5.

Table 2. Boundary conditions of gas suspension calciner for A/F 22.8.

Name of the inlet boundary	Mass flowrate (kg/s)	Temperature (°C)
Air inlet to calciner	47.15	650
Hydrate inlet to calciner	48.88	300
HFO inlet from burners	2.07	115

Table 3. Boundary conditions of gas suspension calciner for A/F 26.5.

Name of the inlet boundary	Mass flowrate (kg/s)	Temperature (°C)
Air inlet to calciner	51.38	650
Hydrate inlet to calciner	46.38	300
HFO inlet from burners	1.956	115

2.3. Fluid-bed Status Graph

Quantification of calcined alumina particles after the calcination process using fluid-bed status graph is very important to understand the effect of retention time-temperature-particle size on product quality (α-alumina) and also identify the fluidization behavior of alumina particles inside calciner and holding vessel. A proper fluidization is essential in an alumina calcination process to obtain desirable product quality in terms of γ-alumina and LOI.

Several researchers have deep dived in fluidization phenomena and have proposed several types of fluidization. Fluidization is a key factor in the current setup of a gas suspension calciner due to its effect on retention time which is crucial in maintaining LOI and consistent alumina quality. Proper fluidization in calciner also opens up the scope for optimization of fuel oil consumption and reduce the undesirable alpha content in final smelter grade alumina [9].

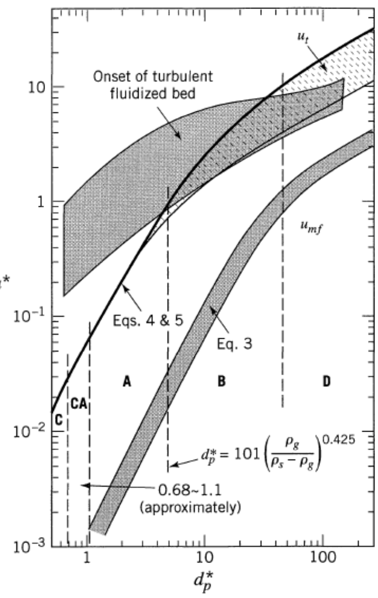

Figure 4. Fluid-bed status graph between dimensionless particle size and dimensionless velocity [10].

The main principle behind fluidization is that, when air is passed upward through a bed of alumina particles, a pressure drop build-up due to the generation of friction. Upon increase in the air velocity, the pressure drop increases until it reaches the weight equivalent to the load of alumina particles upon the cross-sectional area. This velocity is called minimum fluidization velocity (u_{mf}) as shown in Figure 4. At the minimum fluidization velocity [10], all the alumina particles will be observed to suspend, rotate across the cross section of bed, more or less uniformly. When the air velocity exceeds the minimum fluidization velocity, pressure drop exceeds the weight of alumina particles and they would be observed in the state of suspension. This corresponding gas velocity at suspension is given by,

$$150\left(1-\epsilon_{mf}\right)u_{mf}^{*}+1.75\left(u_{mf}^{*}\right)^{2}*d_{p}^{*}=\epsilon_{mf}^{3}\left(d_{p}^{*}\right)^{2} \tag{22}$$

For a further increment in the air velocity above u_{mf}, expansion of all particles which were together is observed until a stage which is called the terminal velocity, u_t. Figure 5 shown below depicts the particles at different velocity regimes.

3. Results and Discussion

3.1. Combustion Analysis

Flow pattern and combustion analysis was performed and investigated in a 3D model of the calciner furnace along with the holding vessel. CFD analysis was carried out for two different air to fuel ratios of 22.8 and 26.5 for different feed rates of alumina hydrate and flow rates of air and HFO. Overall combustion efficiency was found to be good in which HFO was completely combusted with air after the burner zone. Mass fractions of CO_2 and CO show the conversion of HFO to combustion products while the O_2 leaving the holding vessel outlet is the excess air which varies with the variation in air to fuel ratio.

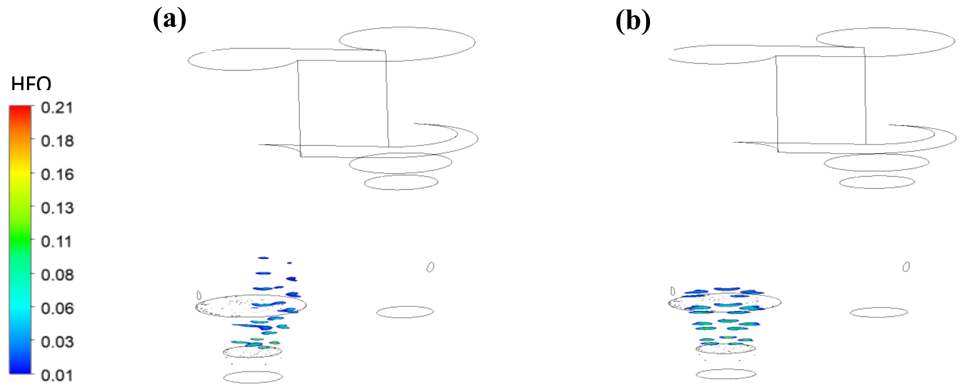

Figure 5. Mass fraction of HFO inside the calciner and holding vessel for (a) A/F – 22.8, (b) A/F - 26.5.

Figure 5-7 depicts the predicted mass fraction distributions of HFO, CO_2 and CO respectively. The fuel oil distribution at lower A/F ratio is found to be biased against the uniform cross-sectional distribution of fuel at higher A/F ratio (Figure 5). Even though the CO2 concentration variation is found in the calciner section, the CO_2 gas is found to be uniformly distributed in the holding vessel section for both the A/F ratios (Figure 6). Nevertheless, CO gas is found to be at higher levels for lower A/F ratios against higher A/F ratio (Figure 7). The mass fractions of all combustion products in the holding vessel outlet was on higher side with excess oxygen for lower A/F 22.8, while, A/F 26.5 had a slightly lower combustion product mass fraction. The higher CO mass fraction in lower A/F ratio is mainly due to the channeling of flue gases from calciner to holding vessel due to biased flow. More gas sensors are being deployed in the calcination plant to validate the composition of gases at different locations of the circuit.

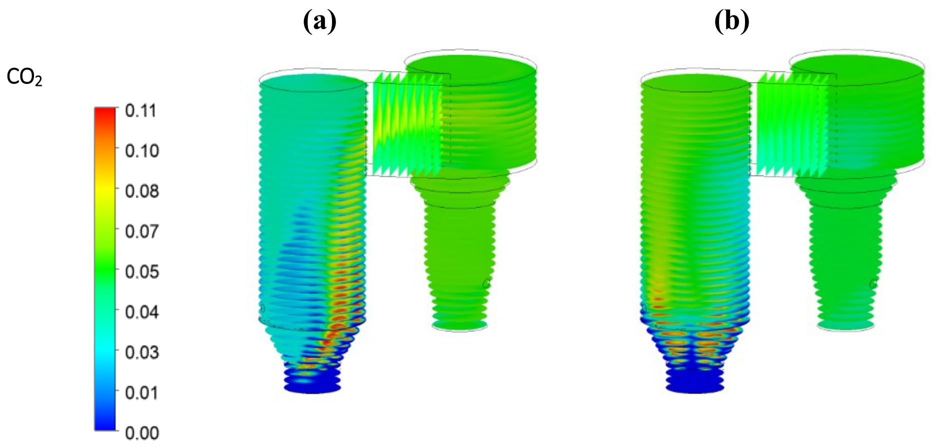

Figure 6. Mass fraction of CO_2 inside the calciner and holding vessel for (a) A/F-22.8 and (b) A/F-26.5.

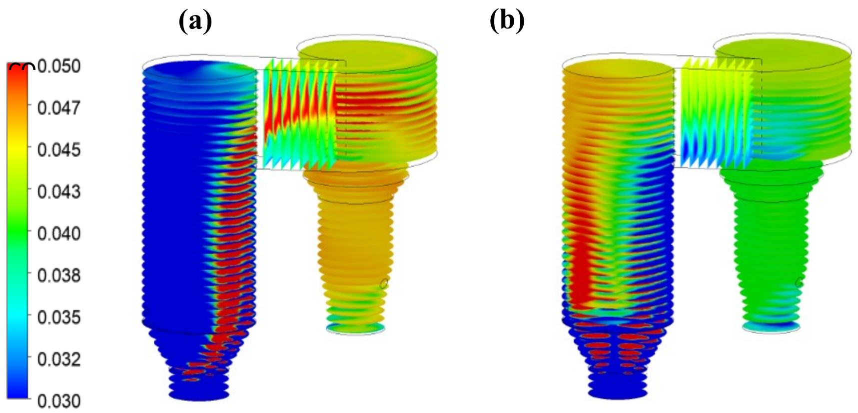

Figure 7. Mass fraction of CO inside the calciner and holding vessel for (a) A/F – 22.8 and (b) A/F 26.5.

3.2. Flow Pattern and Temperature Analysis

Figure 8 depicts the velocity vectors of incoming air carrying alumina particles for air to fuel ratios (A/F) of 22.8 and 26.5. The ratio of air flowrate to hydrate feed rate (A/H) were maintained to be 0.96 and 1.1 respectively for A/F – 22.8 and 26.5.

From the velocity vectors, it was clearly observed that in A/F – 22.8, recirculation's were found to be higher with low velocities in comparison to A/F 26.5. A biased channeling flow on one side of the calciner for A/F 22.8 was observed while a more uniform flow instead of any channeling was observed for A/F 26.5. A channeling flow with bias on one side (A/F 22.8) would create uneven distribution of fuel and air mixing whereas the A/F 26.5 predicted better uniform flow pattern at the entrance of the calciner section. This non-biased uniform swirl mixing phenomenon at higher A/F ratio helped in better fuel oil distribution and in turn would impact the mixing and variation in temperature distribution inside the calciner.

Figure 9 shows the particle track streamlines both in the calciner and holding vessel sections. At lower A/F ratio, particles did experience lower velocity along with larger axial recirculation pattern (Figure 9a) whereas the particles at higher A/F ratio experienced uniform axial upward flow with smaller recirculation zone especially near to the top section of the calciner (Figure 9b). However, in both the A/F ratios, the particle track in the holding vessels are found to be similar with swirl flow pattern.

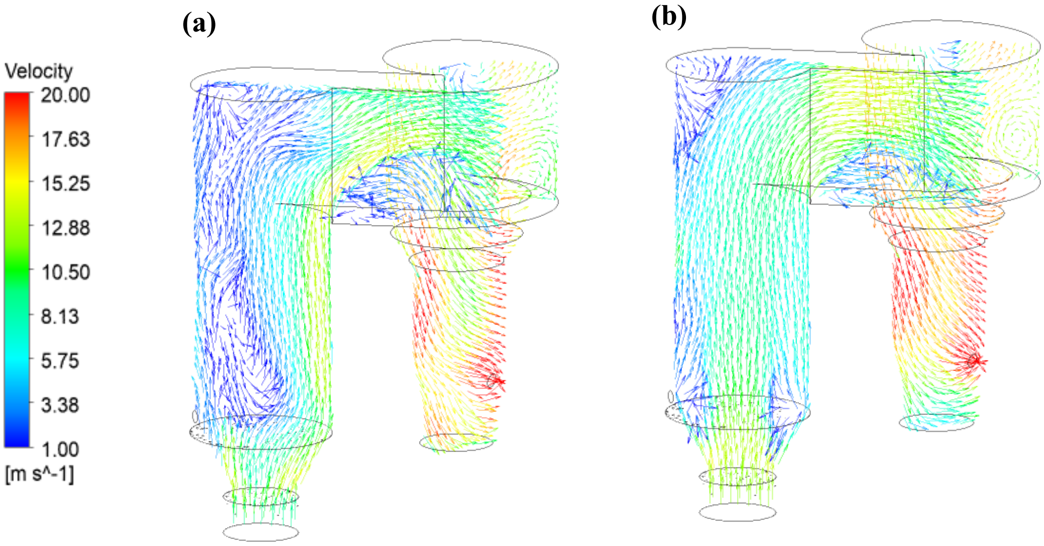

Figure 8. Flow patterns and velocity distributions for (a) A/F – 22.8 and (b) A/F – 26.5.

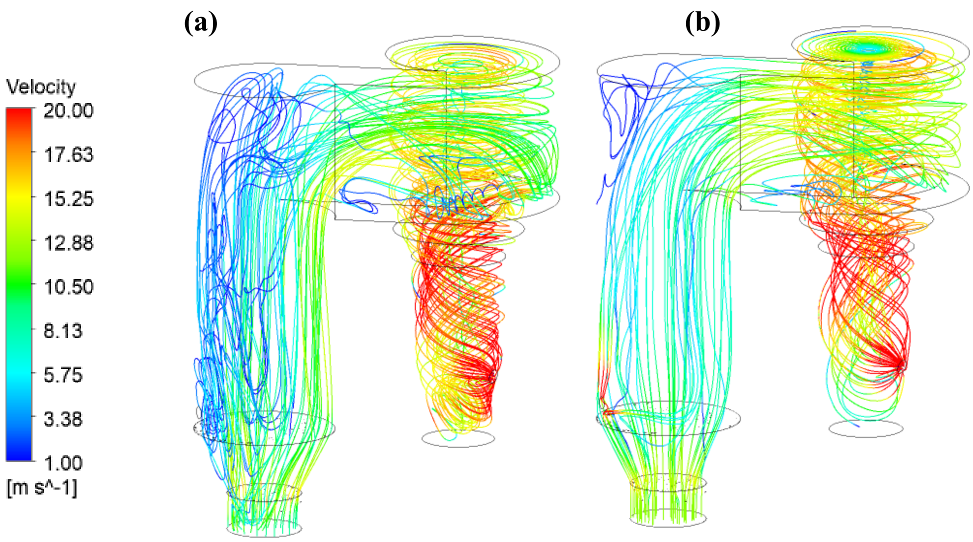

Figure 9. Streamlines for (a) A/F – 22.8 and (b) A/F – 26.5.

Figure 10 depicts the temperature profiles of stream of hydrate/alumina particles with excess air and combustion gases passing through the calciner and holding vessel for different variations of air to fuel ratios. At lower A/F ratio (22.8), due to a biased channeling flow pattern and uneven mixing of fuel oil and air near the location of fuel injection zone, the higher temperature (>1300°C) predictions were observed on one side of the calciner, while the other portions of calciner were maintained between 1000 to 1150°C along the length of the calciner (Figure 10a). Even though, the holding vessel is dominated by swirly flow, the mixing of high temperature biased channeled gases from the calciner section drastically increased the overall temperature in the holding vessel, which varied from 1200 to 1300°C. At higher A/F ratio (Figure 10b), the flow of fuel oil and air did experience a swirl mixing near the burner section, which in turn enhanced the local combustion efficiency near the fuel injection zone and hence the temperature is found to be uniformly distributed across the cross section near the burner region. Further, a gradual and uniform reduction in temperature gradient was observed right from calciner inlet section till the outlet section of the holding vessel.

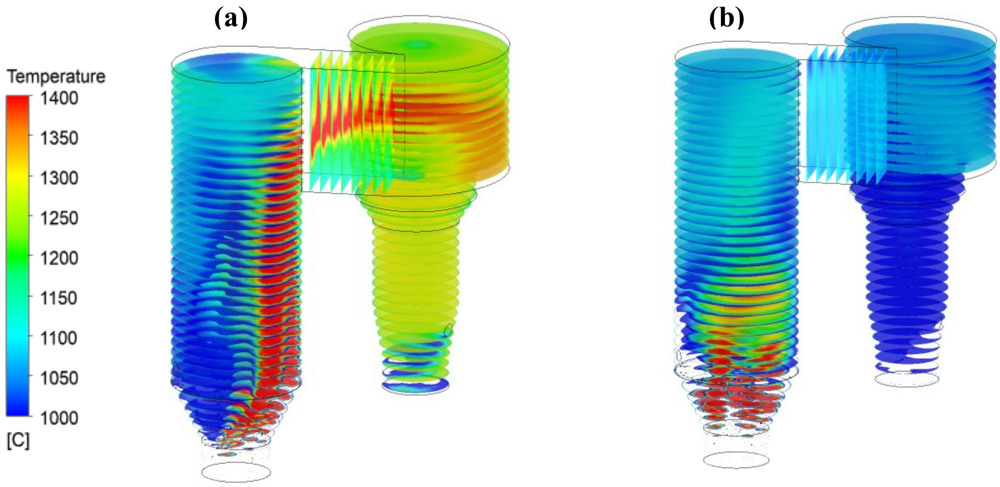

Figure 10. Temperature isoclips in calciner and holding vessel for (a) A/F – 22.8 and (b) A/F – 26.5.

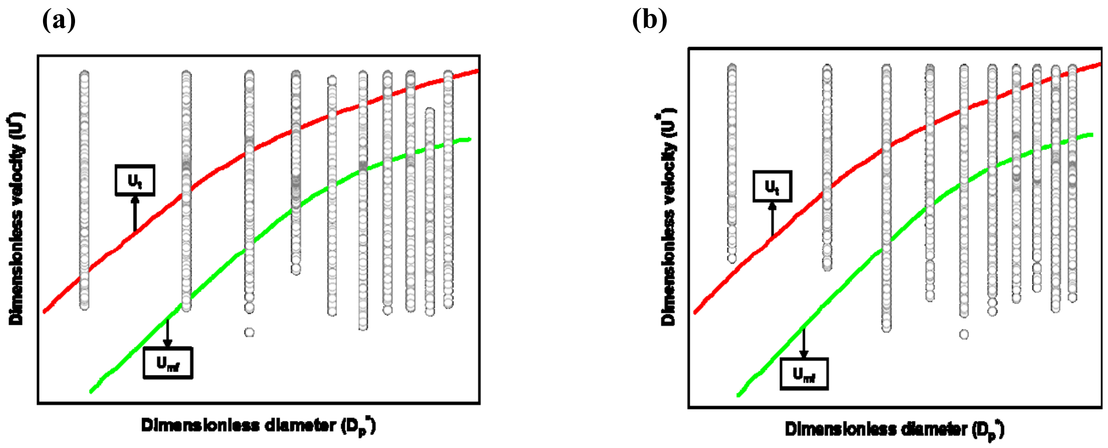

Figure 11. Fluid bed status graph of alumina particles for (a) A/F – 22.8 and (b) A/F – 26.5 at above terminal velocity (Red line), above and below minimum fluidization velocity (Green line).

3.3. Fluidization Studies

It is necessary to quantify the amount of alumina particles spending certain retention time at temperatures greater than 1000°C. Hence, it is important to understand the effect of gas-solid fluidization phenomena along with the particle velocity, size and retention time. For this purpose, the predicted particle size and velocity through CFD analysis was plotted with the fluid-bed status graph developed by O. Levenspiel [10] as shown in Figure 11.

Figure 11 shows the fluid-bed status graph to extract information of particles at different velocity regimes viz., above terminal settling velocity, between terminal and minimum fluidization and less than minimum fluidization velocity. It was observed that for a higher A/F (22.8) where recirculation's were higher, slightly higher number of particles were found to be in the fluidization regime. From the lab scale XRD analysis, it was identified that particle sizes (<75 μ) had a higher tendency to form alpha phase from desirable γ-alumina. The aluminium hydrate sample were collected from the inlet to calcination circuit and experimented in a laboratory muffle furnace for different sets of temperature and heating rate before carrying out XRD analysis. For the sake of brevity, details of XRD results are not shown in this work. Hence, for the quantification study, retention times of finer fractions of alumina particles (<75 μ) in each velocity regime at higher temperatures (>1000 °C) were extracted [11]. Using the lab scale predictions by C.P. Steiner et al., (1971) [12], analysis was carried out to segregate particles spending time in temperatures greater than 1000 °C to understand and validate possible chance for alpha phase formation. It was particularly noticed that when a finer fraction of particles (<75 μ) spends time inside calciner and holding vessel at higher temperatures (>1000 °C), chances to form α-alumina are greater due to an enhanced heat transfer and shorter diffusion distance for reaction products for finer particles to further transform into undesirable α-alumina. From the literature by C.P. Steiner et al., (1971), a linear dependency between percentage of alpha alumina and retention time was observed following zero-order kinetics [12]. Thus, the correlation for alpha content with temperature and residence time was used to understand and validate the formation of alpha alumina from CFD simulations. Table 4 shows the quantitative results in which correlation of percentage alpha phase with retention times spent by alumina particles at three velocity regimes and at a temperature 1000 °C was depicted. The predictions of alpha phase by mapping CFD flow pattern results along with the lab scale phase transformation experiments was found to be in good agreement with plant data (Table 4).

Table 4. Quantitative particle information from CFD analysis.

Air to Fuel	Velocity Zone	Temperature (%)	Retention time (sec)	% Particle size (<75μ)	Actual alpha content	Alpha from simulation
22.8	Above terminal velocity	T between 1000 - 1100	10-40	4.5	5.97	5.58
		T > 1100	15-150			
	Between terminal & minimum fluidization	T between 1000 - 1100	10-60	0.9		
		T > 1100	50 -350			
	Below minimum fluidization	T between 1000 - 1100	15-145	0.2		
		T > 1100	30-430			
		T > 1100	30 - 430			
26.5	Above terminal velocity	T between 1000 - 1100	4-15	0.6	4.24	4.33
		T > 1100	2-12			
	Between terminal & minimum fluidization	T between 1000 - 1100	4-20	2		
		T > 1100	4 -70			
	Below minimum fluidization	T between 1000 - 1100	5-20	0.3		
		T > 1100	10-700			

4. Conclusions

The present study mainly focused on the detailed investigation pertaining to calciner and holding vessel section. CFD analysis was carried out to understand the flow phenomena of gas-solid hydrodynamics along with the distribution of temperature predicted. Along with that, fluidization analysis was carried out to understand the particle retention time and velocity and its effect on alpha phase transformation.

1. The lower A/F ratio (22.8) demonstrated a biased flow pattern with non-uniform mixing pattern leading to poor combustion efficiency in the calciner section whereas the higher A/F ratio (26.5) predicted a non-biased flow pattern with good swirl flow mixing of fuel oil and air leading to better combustion efficiency.
2. The non-biased flow in the higher A/F ratio (26.5) along with the effective combustion of fuel predicted a uniform reduction in temperature gradient starting from the calciner entry till the holding vessel exit.
3. The non-biased flow in the higher A/F ratio (26.5) reduced the recirculation vortices and thus in turn provides an optimum retention time for the desired phase transformation of particles.
4. The biased flow in the lower A/F ratio (22.8) and non-biased flow in the higher A/F ratio (26.5) produced alpha phase formation by ~6 % and ~4.5 % respectively. A difference of 1.5 % was identified between two A/F ratios.

5. Future Work

1. The present work was limited to combustion and holding vessel zones of gas suspension calciner. CFD simulation of the whole gas suspension calciner unit, which includes cooling cyclones and pre-heater sections would be carried out for optimization of Heavy fuel oil (HFO) consumption for different variations of feed rates.

2. In the upcoming CFD simulations, both SO_x and NO_x reactions will be included.

6. References

1. K. Wefers and M. Chanakya, Oxides and hydroxides of aluminum, Pittsburgh: *Alcoa Laboratories*, 1987.
2. I. Jones, J. Victoria, C. S. Robert, D. Thomas, W.S.C. Jennifer, and S. Sylvain, Dehydroxylation sequences of gibbsite and boehmite: study of differences between soak and flash calcination and of particle-size effects., *Journal of Materials Chemistry,* Vol. 6, No. 1, pp. 73-79, 1996.
3. J. A. Jiménez, P. Isabel , L. Aurora , F. Laila and L. Sol , Characterization of the aluminas formed during the thermal decomposition of boehmite by the rietveld refinement method., *International Journal of Applied Ceramic Technology,* Vol. 12, pp. 178-186, 2015.
4. C. Marsh, "CFD Modelling of Alumina Calciner Furnaces," *CSIRO Australia,* pp. 9-11, 2009.
5. D. J. Gunn, Transfer of heat or mass to particles in fixed and fluidised beds., *International Journal of Heat and Mass Transfer,* Vol. 21, No. 4, pp. 467-476, 1978.
6. S. Morsi and A. J. Alexander, An investigation of particle trajectories in two-phase flow systems., *Journal of Fluid mechanics,* Vol. 55, No. 2, pp. 193-208, 1972.
7. C. L. Wu, K. Nandakumar, A. S. Berrouk and H. Kruggel-Emden, Enforcing mass conservation in DPM-CFD models of dense particulate flows., *Chemical engineering journal,* Vol. 174, No. 1, pp. 475-481, 2011.
8. Versteeg, K. Henk and M. Weeratunge , An introduction to computational fluid dynamics: the finite volume method., Pearson education, 2007.

9. T. Kumaresan, S. Thakre, B. Basu, B. Jain, K. Pandey, R. Singh and R. Somani, Design Optimization of the De-duster to reduce Alumina carry over load on the dry scrubbing system, *International Conference on CFD in Oil & Gas, Metallurgical and Process Industries*, Trondheim, Norway, 2008.
10. O. Levenspiel, Chemical reaction engineering, *Industrial & engineering chemistry research,* Vol. 38, No. 11, pp. 4140-4143, 1999.
11. O. Levenspiel, Chemical Reaction Engineering, New York, NY: Wiley, 1999.
12. C. P. Steiner, D. Hasselman and R. M. Spriggs, Kinetics of the Gamma-to-Alpha Alumina Phase Transformation, *Journal of American Ceramic Society,* Vol. 54, No. 8, pp. 412-413, 1971.